Cramer-Rao lower bound on wavefront sensor error

Jack Cederquist, MEMBER SPIE
S. R. Robinson
D. Kryskowski
J. R. Fienup, MEMBER SPIE
C. C. Wackerman
Environmental Research Institute
of Michigan
P.O. Box 8618
Ann Arbor, Michigan 48107

Abstract. Wavefront sensors that can operate at low light levels, be built from present technology components, and provide accurate wavefront phase estimates in real time are required for use with adaptive optics systems. The use of estimation theory makes possible the evaluation of wavefront sensors without specification of the wavefront phase estimation algorithms. The Cramer-Rao method was used to find a lower bound on integrated rms wavefront sensor estimation error. In addition to an analysis of the general case, the error lower bound was numerically evaluated for the shearing interferometer wavefront sensor. Computer simulations of the atmosphere and wavefront sensor measurements including noise were performed. Using an appropriate algorithm, the phase was estimated and the resulting phase error was compared with the lower bound. The results support the validity of using the Cramer-Rao lower bound to evaluate wavefront sensor performance.

Subject terms: wavefront sensors; Cramer-Rao lower bound; shearing interferometer.

Optical Engineering 25(4), 586-592 (April 1986).

CONTENTS

1. INTRODUCTION

A number of sensors that measure wavefront aberrations due to atmospheric turbulence or optical system misalignment are in various stages of development. Most sensors measure the effect of the aberrations on some intensity distribution and seek to infer, via data processing, the aberrations from the measured intensity. Different types of measurements are made and different algorithms are used to estimate the wavefront phase for each sensor. The tasks of evaluating the performance of a given sensor-algorithm combination or developing a new sensor concept are difficult. A worthy goal, then, is to develop a technique by which wavefront sensor designs may be more easily evaluated.

Paper 2155 received July 8, 1985; revised manuscript received Dec. 23, 1985; accepted for publication Dec. 23, 1985; received by Managing Editor Dec. 31, 1985. This paper is a revision of Paper 551-06 which was presented at the SPIE conference on Adaptive Optics, April 10–11, 1985, Arlington, Va. The paper presented there appears (unrefereed) in SPIE Proceedings Vol. 551.

In this paper, the use of Cramer-Rao lower bounds on the integrated rms phase estimate error as a technique for wavefront sensor design and analysis is described. In Sec. 2, a mathematical model of the wavefront sensing process is given. The Cramer-Rao method is applied, in the general case, in Sec. 3. A specific wavefront sensor is analyzed in Sec. 4. The usefulness of the Cramer-Rao approach is demonstrated in Sec. 5 by comparison of the error lower bound to the phase estimate error obtained by computer simulation. Conclusions and suggestions for further work are given in Sec. 6.

2. WAVEFRONT SENSOR MODEL

The wavefront sensor receives the electromagnetic field from an object after it has acquired a phase aberration. To maintain generality, the object is allowed to be extended and the field is of arbitrary coherence. It will, however, be assumed that the field (emitted by or scattered from the object) is quasi-monochromatic and that the distance between the object and the sensor is sufficiently great that the Fraunhofer approximation can be made. The field is therefore characterized by its mutual intensity $M(\mathbf{x}, \mathbf{y})$ in the sensor input aperture in the absence of any phase aberration. ($\mathbf{x}$ and other boldface symbols will denote two-dimensional vectors.) The phase aberration will be assumed to be isoplanatic and given by the function $\phi(\mathbf{x})$.

The intensity at the detector is[1]

$$I(\mathbf{u}) = \int_A \int_A h(\mathbf{u}, \mathbf{x}) h^*(\mathbf{u}, \mathbf{y}) M(\mathbf{x}, \mathbf{y}) \exp\{i[\phi(\mathbf{x}) - \phi(\mathbf{y})]\} d\mathbf{x} d\mathbf{y} , \quad (1)$$

where $h(\mathbf{u}, \mathbf{x})$ is the coherent impulse response of the sensor and A is the region defined by the sensor aperture. A linear detector is assumed, and the detected signal is

$$s(\mathbf{u}) = \eta T I(\mathbf{u}) + n(\mathbf{u}) , \quad (2)$$

where η is the quantum efficiency of the detection process, T is the detector integration time, and $n(\mathbf{u})$ is additive noise. It is assumed that T is long compared to the time over which the field must be averaged to give the mutual intensity, but short compared to the time required for the atmospheric phase to change significantly.

Further modeling of the detector signal as a discrete signal

$$s_j = \int_{P_j} s(\mathbf{u})d\mathbf{u} , \tag{3}$$

where P_j is the *jth* detector element, is possible, but is avoided here for simplicity. However, in Sec. 5 theoretical results are interpreted and applied to the case of discrete signals.

3. APPLICATION OF CRAMER-RAO METHOD

The phase estimation problem is one of determining $\hat{\phi}(\mathbf{x})$, an estimate of the phase $\phi(\mathbf{x})$, from the measurements $s(\mathbf{u})$. The goal in this section is to find a lower bound on the error of the estimate $\hat{\phi}(\mathbf{x})$, given knowledge of (1) the properties of the wavefront sensor and (2) the statistics of $\phi(\mathbf{x})$ and the noise $n(\mathbf{u})$. The Cramer-Rao method will be applied to the wavefront sensor model described in Sec. 2. A first step in this direction is described in Ref. 2 and is based on the extension of Cramer-Rao bounds to continuous signals as developed in Ref. 3. The discussion in this section will state assumptions, give new and corrected results, and provide interpretations for limiting cases. The reader is referred to Ref. 4 for an excellent tutorial on the Cramer-Rao method.

For application to wavefront sensing, the following assumptions will be made: (1) The phase $\phi(\mathbf{x})$ is a sample function from a zero mean Gaussian random process with covariance

$$E[\phi(\mathbf{x})\,\phi(\mathbf{y})] = K(\mathbf{x} - \mathbf{y}) , \tag{4}$$

where $E[\cdot]$ signifies expected value. (2) The noise $n(\mathbf{u})$ is a sample function from a zero mean Gaussian random process with covariance

$$E[n(\mathbf{u})n(\mathbf{v})] = \frac{N}{2}\delta(\mathbf{u} - \mathbf{v}) . \tag{5}$$

(3) The estimate $\hat{\phi}(\mathbf{x})$ of the phase is unbiased, which is equivalent to

$$E[\hat{\phi}(\mathbf{x}) - \phi(\mathbf{x})] = 0 . \tag{6}$$

Note that these assumptions are stricter than required by the Cramer-Rao method. In particular, the phase covariance need not be stationary, and the noise need not be white.

3.1. Lower bound on estimation error

The integrated mean-squared error of the phase estimate is

$$e^2 = \frac{1}{A}\int_A E\{[\hat{\phi}(\mathbf{x}) - \phi(\mathbf{x})]^2\}d\mathbf{x} , \tag{7}$$

where A is interpreted as the area of the sensor input aperture. It can be proven that e^2 has a lower bound e_0^2 given by[4]

$$e_0^2 = \frac{1}{A}\int_A J^{-1}(\mathbf{x}, \mathbf{x})d\mathbf{x} . \tag{8}$$

The inverse information kernel $J^{-1}(\mathbf{x},\mathbf{x})$ can be shown to be related to the known quantities by the integral equation

$$J^{-1}(\mathbf{x}, \mathbf{y}) + \int_A\int_A J^{-1}(\mathbf{x}, \mathbf{p})R(\mathbf{p}, \mathbf{q})K(\mathbf{q} - \mathbf{y})d\mathbf{p}d\mathbf{q} = K(\mathbf{x} - \mathbf{y}) , \tag{9}$$

where

$$\begin{aligned} R(\mathbf{x}, \mathbf{y}) = {} & \frac{4\eta^2T^2}{N}\exp[-2K(\mathbf{0})] \\ & \times \mathrm{Re}\int_P\int_A\int_A h(\mathbf{u}, \mathbf{x})h^*(\mathbf{u}, \mathbf{p})M(\mathbf{x}, \mathbf{p})\exp[K(\mathbf{x} - \mathbf{p}) + K(\mathbf{y} - \mathbf{q})] \\ & \times \{h^*(\mathbf{u}, \mathbf{y})h(\mathbf{u}, \mathbf{q})M^*(\mathbf{y}, \mathbf{q}) \\ & \times \exp[K(\mathbf{x} - \mathbf{y}) - K(\mathbf{x} - \mathbf{q}) - K(\mathbf{y} - \mathbf{p}) + K(\mathbf{p} - \mathbf{q})] \\ & - h(\mathbf{u}, \mathbf{y})h^*(\mathbf{u}, \mathbf{q})M(\mathbf{y}, \mathbf{q}) \\ & \times \exp[-K(\mathbf{x} - \mathbf{y}) + K(\mathbf{x} - \mathbf{q}) + K(\mathbf{y} - \mathbf{p}) - K(\mathbf{p} - \mathbf{q})]\} \\ & d\mathbf{u}d\mathbf{p}d\mathbf{q} \end{aligned} \tag{10}$$

and P is the region in the $\mathbf{u}$-plane where the intensity is detected.

3.2. Lower bound for limiting cases

To aid in the intuitive understanding of these results, consider two limiting cases: (1) a sensor with very poor detected-signal-to-noise ratio and (2) a sensor that detects only the intensity in the aperture (a poor choice of measurement since it gives no phase information). It would be expected that in either case the error e^2 will approach the error of a phase estimate based on a priori information only (i.e., the measurement gives no information). Since the phase is assumed to be zero mean, this error is $K(\mathbf{0}) \equiv \sigma_\phi^2$, the phase variance.

The Cramer-Rao lower bound e_0^2 for these two cases can be evaluated easily if the mutual intensity $M(\mathbf{x}, \mathbf{y})$ is assumed to be a constant I (i.e., the object is a point). Case (1) corresponds to $I^2/N \to 0$ and case (2) to $h(\mathbf{u}, \mathbf{x}) = \delta(\mathbf{u} - \mathbf{x})$. Examination of Eq. (10) indicates that $R(\mathbf{x}, \mathbf{y}) \to 0$ in both cases. The solution of Eq. (9) is then $J^{-1}(\mathbf{x}, \mathbf{y}) = K(\mathbf{x} - \mathbf{y})$, and Eq. (8) gives $e_0^2 = \sigma_\phi^2$. This agrees with the intuitive reasoning given above.

3.3. Further assumptions and development

Since many wavefront sensors use multiple measurement planes, it is necessary to extend these results. Suppose there are m measurement planes with corresponding impulse responses $h_j(\mathbf{u}, \mathbf{x})$, $j = 1, \ldots, m$. (These impulse responses are assumed to be normalized in such a way that total energy is conserved in the sensor.) The detected signals are then

$$s_j(\mathbf{u}) = \eta T I_j(\mathbf{u}) + n_j(\mathbf{u}) , \quad j = 1, \ldots, m . \tag{11}$$

Assuming the noises n_j are statistically independent and

$$E[n_j(\mathbf{u})n_j(\mathbf{v})] = \frac{N_j}{2}\delta(\mathbf{u} - \mathbf{v}) , \tag{12}$$

then it is straightforward to show that

$$R(\mathbf{x}, \mathbf{y}) = \sum_{j=1}^{m} R_j(\mathbf{x}, \mathbf{y}) , \tag{13}$$

where $R_j(\mathbf{x}, \mathbf{y})$ is given by Eq. (10) using $h_j(\mathbf{u}, \mathbf{x})$.

The solution of the integral Eq. (9) is a difficult task. The numerical results reported in Sec. 4 are based on an approximate solution applicable when $R(\mathbf{x}, \mathbf{y}) = R(\mathbf{x} - \mathbf{y})$ (i.e., R is shift-invariant). Equation (9) is then

$$J^{-1}(\mathbf{x} - \mathbf{y}) + \int_A\int_A J^{-1}(\mathbf{x} - \mathbf{p})R(\mathbf{p} - \mathbf{q})K(\mathbf{q} - \mathbf{y})d\mathbf{p}d\mathbf{q} = K(\mathbf{x} - \mathbf{y}) . \tag{14}$$

Approximating the integrals over the sensor aperture A by infinite limit integrals and Fourier transforming gives

$$\tilde{J}^{-1}(\mathbf{f}) + \tilde{J}^{-1}(\mathbf{f})\tilde{R}(\mathbf{f})\tilde{K}(\mathbf{f}) = \tilde{K}(\mathbf{f}) , \tag{15}$$

where

$$\tilde{F}(\mathbf{f}) = \int F(\mathbf{x}) \exp(-i2\pi\mathbf{x}\cdot\mathbf{f}) \, d\mathbf{x} . \tag{16}$$

The solution is

$$\tilde{J}^{-1}(\mathbf{f}) = \frac{\tilde{K}(\mathbf{f})}{1 + \tilde{R}(\mathbf{f})\tilde{K}(\mathbf{f})} , \tag{17}$$

and the lower bound is

$$e_0^2 = \frac{1}{A}\int_A J^{-1}(\mathbf{0}) \, d\mathbf{x} = J^{-1}(\mathbf{0}) = \int \tilde{J}^{-1}(\mathbf{f}) \, d\mathbf{f} . \tag{18}$$

An important insight here is to note that the lower bound e_0^2 will be minimized if $\tilde{R}(\mathbf{f})$ is large wherever $\tilde{K}(\mathbf{f})$ is large.

In the analysis of a specific wavefront sensor in Sec. 4, it will be assumed that the form of the atmospheric phase covariance is

$$K(\mathbf{x} - \mathbf{y}) = \sigma_\phi^2 \exp\left(\frac{-|\mathbf{x} - \mathbf{y}|^2}{r_\phi^2}\right) , \tag{19}$$

where r_ϕ is the correlation length of the phase and, as noted above, σ_ϕ^2 is the phase variance. These parameters can be related to the commonly used atmospheric coherence length r_0 (Ref. 5) using standard formulas.[6] It can be shown that $r_0 \propto r_\phi/\sigma_\phi$, where the proportionality constant is approximately 1.86. For later use, the Fourier transform of $K(\mathbf{x} - \mathbf{y})$ is

$$\tilde{K}(\mathbf{f}) = \pi r_\phi^2 \sigma_\phi^2 \exp\left(-\pi^2 r_\phi^2 f^2\right) . \tag{20}$$

It will also be assumed that the extended object is incoherent and has a Gaussian intensity distribution. The mutual intensity is

$$M(\mathbf{x}, \mathbf{y}) = I \exp\left(\frac{-|\mathbf{x} - \mathbf{y}|^2}{l^2}\right) , \tag{21}$$

where I is the intensity and l is the field coherence length in the sensor aperture.

4. LOWER BOUND FOR A SHEARING INTERFEROMETER

The shearing interferometer in various forms has been widely studied and used as a wavefront sensor.[7–9] This fact alone is a sufficient reason to investigate its Cramer-Rao error bound, but the discussion here will also be used to illustrate and motivate the use of the Cramer-Rao method.

The shearing interferometer operates by dividing the incoming wavefront into two parts, spatially shifting one part in a shear direction $\mathbf{d}_k$, recombining the two parts with a constant phase difference Δ_j, and detecting the resulting interference pattern. Using temporal (ac heterodyne) and/or spatial (multiple interferometer) multiplexing, this operation is performed for orthogonal shears $\mathbf{d}_1$ and $\mathbf{d}_2$ and for multiple phase differences $\Delta_j = j\pi/2$, $j = 1, 2, 3, 4$, within a time period no greater than the coherence time of the phase aberration $\phi(\mathbf{x})$. (The version of the shearing interferometer considered here requires eight measurement planes. Versions using phase differences $\Delta_j = j2\pi/3$, $j = 1, 2, 3$, and therefore requiring six measurements are also possible.)

The impulse response of the sensor is therefore

$$h_{jk}(\mathbf{u}, \mathbf{x}) = \frac{1}{4\sqrt{2}}\left[\delta(\mathbf{u} - \mathbf{x}) + \exp\left(\frac{ij\pi}{2}\right)\delta(\mathbf{u} - \mathbf{x} + \mathbf{d}_k)\right] , \quad j = 1, 2, 3, 4; \quad k = 1, 2 . \tag{22}$$

The factor $1/(4\sqrt{2})$ provides for conservation of energy. Using Eq. (1), the intensity to be detected is

$$I_{jk}(\mathbf{u}) = \frac{1}{32}\left\{M(\mathbf{u}, \mathbf{u}) + M(\mathbf{u} + \mathbf{d}_k, \mathbf{u} + \mathbf{d}_k) + 2|M(\mathbf{u}, \mathbf{u} + \mathbf{d}_k)| \times \cos\left[\phi(\mathbf{u} + \mathbf{d}_k) - \phi(\mathbf{u}) + \frac{j\pi}{2} + \arg M(\mathbf{u}, \mathbf{u} + \mathbf{d}_k)\right]\right\} , \quad j = 1, 2, 3, 4; \quad k = 1, 2 . \tag{23}$$

From these measurements, the wavefront slope $\phi(\mathbf{u} + \mathbf{d}_k) - \phi(\mathbf{u})$ may be found, provided the mutual intensity M can be eliminated. An excellent algorithm for computing the least mean-squared error phase estimate from the wavefront slope data is the method of successive overrelaxation.[10]

4.1. Point object case

It is useful to start with the point object case for which $M(\mathbf{x}, \mathbf{y}) = I$, a constant. Substituting $h_{11}(\mathbf{u}, \mathbf{x})$ into Eq. (10) and using the delta functions to perform the integrations gives

$$R_{11}(\mathbf{x}, \mathbf{y}) = \frac{\eta^2 T^2 I^2}{256N}(1 + \exp\{-4[K(\mathbf{0}) - K(\mathbf{d}_1)]\}) \times [2\delta(\mathbf{x} - \mathbf{y}) - \delta(\mathbf{x} - \mathbf{y} + \mathbf{d}_1) - \delta(\mathbf{x} - \mathbf{y} - \mathbf{d}_1)] . \tag{24}$$

Note that since R is a function of $\mathbf{x} - \mathbf{y}$, the Fourier domain

solution for $J^{-1}(\mathbf{x} - \mathbf{y})$ from Sec. 3.3 can be used.

It is interesting to qualitatively compare the error bounds for impulse responses $h_{11}(\mathbf{u}, \mathbf{x})$ and $h_{21}(\mathbf{u}, \mathbf{x})$. The corresponding detected intensities are

$$I_{11}(\mathbf{u}) = \frac{I}{16}\{1 - \sin[\phi(\mathbf{u} + \mathbf{d}_1) - \phi(\mathbf{u})]\}, \tag{25}$$

$$I_{21}(\mathbf{u}) = \frac{I}{16}\{1 - \cos[\phi(\mathbf{u} + \mathbf{d}_1) - \phi(\mathbf{u})]\}, \tag{26}$$

and the Fourier transforms of $R(\mathbf{x} - \mathbf{y})$ are

$$\tilde{R}_{11}(\mathbf{f}) = \frac{\eta^2 T^2 I^2}{128N}(1 + \exp\{-4[K(\mathbf{0}) - K(\mathbf{d}_1)]\}) \times [1 - \cos(2\pi\mathbf{f}\cdot\mathbf{d}_1)], \tag{27}$$

$$\tilde{R}_{21}(\mathbf{f}) = \frac{\eta^2 T^2 I^2}{128N}(1 - \exp\{-4[K(\mathbf{0}) - K(\mathbf{d}_1)]\}) \times [1 - \cos(2\pi\mathbf{f}\cdot\mathbf{d}_1)]. \tag{28}$$

$\tilde{R}_{11}(\mathbf{f})$ is greater than $\tilde{R}_{21}(\mathbf{f})$ for all $\mathbf{f}$ because of the plus sign before the exponential. Recalling the comment in Sec. 3.3 that a larger $\tilde{R}(\mathbf{f})$ gives a smaller lower bound on the error, it can be concluded that the sine rather than the cosine measurement of $\phi(\mathbf{u} + \mathbf{d}_1) - \phi(\mathbf{u})$ is more useful from the Cramer-Rao point of view. Especially for small wavefront slopes, this result agrees with common experience and intuition. Note also that, for zero shear distance, both $\tilde{R}_{11}(\mathbf{f})$ and $\tilde{R}_{21}(\mathbf{f})$ are identically zero. This will give a lower bound of σ_ϕ^2, as expected (see Sec. 3.2).

4.2. Extended object case

Substitution of Eq. (22) into Eq. (10) and use of Eq. (13) gives

$$R(\mathbf{x}, \mathbf{y}) = \frac{\eta^2 T^2}{64N}\sum_{j=1}^{2}\sum_{k=1}^{2}|M(\mathbf{x}, \mathbf{x} + (-1)^j\mathbf{d}_k)|^2 \times \{\delta[\mathbf{x} - \mathbf{y}] - \delta[\mathbf{x} - \mathbf{y} + (-1)^j\mathbf{d}_k]\}, \tag{29}$$

where it is assumed that the noise covariance is identical in each measurement plane.

To facilitate use of the Fourier domain solution and further computation, it will be assumed that the mutual intensity is given by Eq. (21) and that $|\mathbf{d}_1|$ and $|\mathbf{d}_2| = d$. (Other less restrictive assumptions can also be made at the expense of increased algebraic and numerical complexity.) The result is

$$\tilde{R}(\mathbf{f}) = \frac{\eta^2 T^2 I^2}{32N}\exp\left(\frac{-2d^2}{l^2}\right) \times [2 - \cos(2\pi\mathbf{f}\cdot d\hat{\mathbf{x}}_1) - \cos(2\pi\mathbf{f}\cdot d\hat{\mathbf{x}}_2)], \tag{30}$$

where $\hat{\mathbf{x}}_1$ and $\hat{\mathbf{x}}_2$ are orthogonal unit vectors. Using Eqs. (17), (18), (20), and (21) gives for the Cramer-Rao lower bound on the phase estimation error

$$e_0^2 = \pi\sigma_\phi^2\int_0^\infty\int_0^{2\pi}\frac{\exp(-\pi^2 f_0^2) f_0 df_0 d\theta}{1 + P_1 C(f_0, \theta)\exp(-\pi^2 f_0^2)}, \tag{31}$$

where

$$C(f_0, \theta) = 2 - \cos\left(\frac{2\pi f_0 d\cos\theta}{r_\phi}\right) - \cos\left(\frac{2\pi f_0 d\sin\theta}{r_\phi}\right), \tag{32}$$

a change of variable $f_0 = r_\phi f$ has been made, and

$$P_1 = \frac{\pi r_\phi^2 \sigma_\phi^2 \eta^2 T^2 I^2}{32N}\exp\left(\frac{-2d^2}{l^2}\right). \tag{33}$$

Parameter P_1 contains the ratio $\eta^2T^2I^2/(N/2)$, which represents the ratio of signal power to thermal noise power. (For the purpose of estimation theory, the signal is ηTI, so the signal power is $\eta^2T^2I^2$.) Since wavefront sensors are often used in low light level conditions, the detectors used should ideally be shot noise limited. It is therefore appropriate to reinterpret P_1 as follows: The number of detected photons per unit area is

$$s = \frac{\eta TI}{h\nu}, \tag{34}$$

where η is the detector quantum efficiency, T is the integration time, I is the intensity in the aperture, and $h\nu$ is the energy of a photon. The associated shot noise power is

$$N_s = \frac{\eta TI}{h\nu}. \tag{35}$$

In Eq. (33), $\eta^2T^2I^2/(N/2)$ should therefore be replaced by

$$\frac{s^2}{N_s} = \frac{\eta TI}{h\nu}. \tag{36}$$

Further simplification is possible by defining an atmospheric coherence cell to be of area πr_ϕ^2 and noting that the number of detected photons per coherence cell in time T is

$$P_c = \frac{\pi r_\phi^2 \eta TI}{h\nu}. \tag{37}$$

For the shot-noise-limited case, the parameter P_1 then becomes

$$P_1 = \left(\frac{\sigma_\phi^2 P_c}{64}\right)\exp\left(\frac{-2d^2}{l^2}\right). \tag{38}$$

For use in Sec. 5, note that the variance σ_N^2 of thermal noise is equal to N/2 by Eq. (5). An alternative expression for P_c, applicable to the thermal-noise-limited case, is therefore

$$P_c = \frac{\pi r_\phi^2 \eta^2 T^2 I^2}{\sigma_N^2}. \tag{39}$$

It is important to note that e_0 depends on only four param-

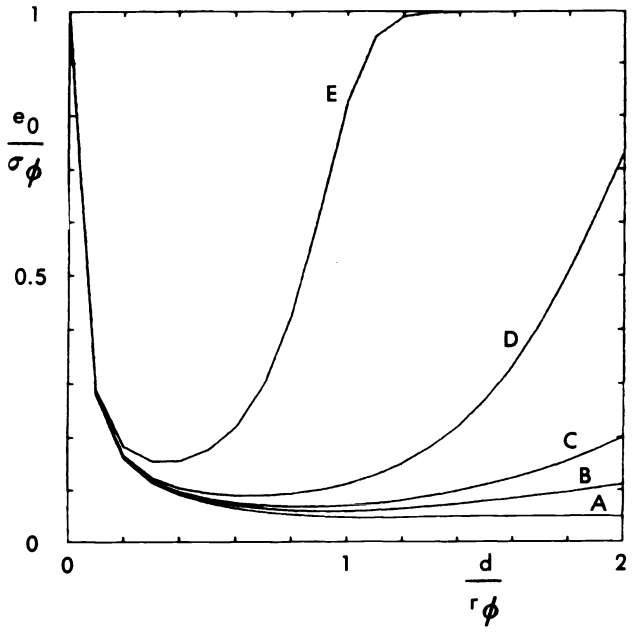

Fig. 1. Shearing interferometer normalized lower bound e_0/σ_ϕ versus ratio of shear distance d to atmospheric correlation length r_ϕ at light level P_c of 10^5 photons per atmospheric coherence cell for rms atmospheric phase $\sigma_\phi = \pi/2$. Curve (A) is for a point object and curves (B) through (E) are for extended objects with ratios of the field coherence length l to r_ϕ of 2, 1.5, 1, and 0.5, respectively. The object for (E) has therefore four times the angular extent of the object for (B). The optimum shear is approximately the smaller of r_ϕ and $l/2$.

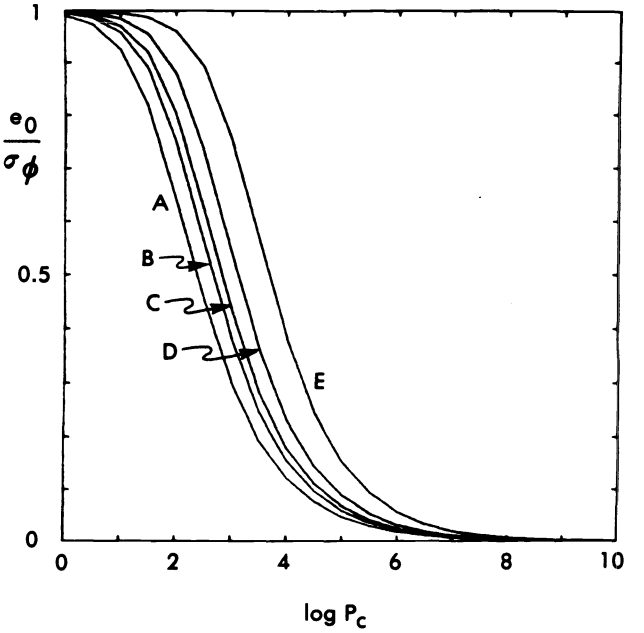

Fig. 2. e_0/σ_ϕ for shearing interferometer versus light level P_c for $\sigma_\phi = \pi/2$. Curve (A) is for a point object and curves (B) through (E) are for extended objects with l/r_ϕ equal to 2, 1.5, 1, and 0.5, respectively. For each curve, the optimum shear d from Fig. 1 is used.

eters: σ_ϕ^2, P_c, l/r_ϕ, and d/r_ϕ. The dependence on these parameters was investigated numerically. Figure 1 shows plots of e_0/σ_ϕ versus d/r_ϕ with $\sigma_\phi = \pi/2$ for various values of l/r_ϕ. For the point object (curve A), a shear d approximately equal to the atmospheric phase correlation length r_ϕ minimizes the lower bound. The lower bound predicts that further increases in the shear do not significantly alter sensor performance. For the extended object, the lower bound is minimized for a shear d of about $l/2$. Further increases in the shear seriously degrade lower bound performance. The minimum lower bound is smaller for the point object case. This behavior is as expected and agrees with other investigations.[9]

The dependence of e_0 on light level and object size is demonstrated in Fig. 2, which shows plots of e_0/σ_ϕ versus P_c with $\sigma_\phi = \pi/2$ and optimum shear from Fig. 1 for various values of l/r_ϕ. As expected, the lower bound decreases with increasing light level and performance degrades as l/r_ϕ decreases.

Figure 3 shows plots of e_0 versus P_c with a point object and near optimum shear $d = r_\phi$ for various values of σ_ϕ. Note that, although absolute performance degrades with increasing σ_ϕ, relative performance (e_0/σ_ϕ) improves. A new prediction, based on this figure, is that at high light levels the absolute performance for large σ_ϕ can approach that for a smaller σ_ϕ. At low light levels, the lower bound for large σ_ϕ becomes significantly worse. Apparently, at high light levels, the finer sampling required to track the large variations in the phase can be achieved without significantly increasing the noise level. At low light levels, this is not possible and the lower bound increases.

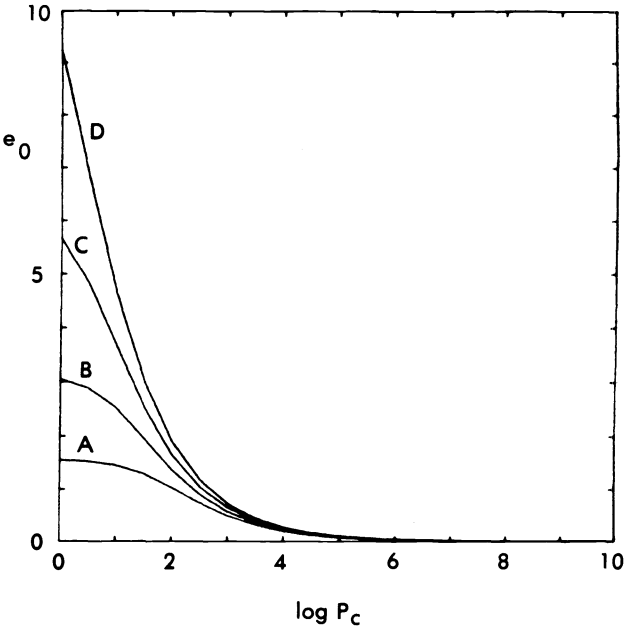

Fig. 3. Shearing interferometer lower bound e_0 versus P_c for a point object and σ_ϕ of (A) $\pi/2$, (B) π, (C) 2π, and (D) 4π. Although relative performance improves as σ_ϕ increases, absolute performance degrades.

5. COMPARISON OF CRAMER-RAO ERROR BOUNDS TO SIMULATED SENSOR-ALGORITHM PERFORMANCE

In Sec. 4, the Cramer-Rao method was used to find a lower bound on the rms phase estimate error for a shearing interferometer wavefront sensor. The Cramer-Rao lower bounds will be useful in evaluating and developing sensor designs only if

they can be related to the actual performance of given combinations of sensors and phase estimation algorithms. To investigate this relationship, a computer simulation of a shearing interferometer with a successive overrelaxation algorithm was performed.

A point object was assumed. The atmospheric phase aberration was simulated by (1) placing uncorrelated, zero mean, unit variance Gaussian distributed random numbers into the real and imaginary parts of a two-dimensional array; (2) filtering the array by multiplication by a modified Kolmogorov spectrum $1/[1 + c^2(j^2 + k^2)]^{11/12}$, where j and k index the rows and columns of the array, element (j, k) = (0, 0) is at the center of the array, and the parameter c determines the correlation length r_ϕ; (3) Fourier transformation and subsequent use of only the real part of the resulting array; and (4) multiplication of the array by an appropriate constant to give an atmospheric phase with a specified variance σ_ϕ^2.[11] Statistical tests have shown that the simulated phase was zero mean and Gaussian distributed. A phase with a Kolmogorov power spectrum has a covariance

$$K(\mathbf{x} - \mathbf{y}) = \sigma_\phi^2 - 3.44\left(\frac{|\mathbf{x} - \mathbf{y}|}{r_0}\right)^{5/3}. \tag{40}$$

As expected,[11] the covariance of the simulated phase was found to decrease less rapidly with $|\mathbf{x} - \mathbf{y}|$ than indicated by Eq. (40). The Gaussian covariance of Eq. (19) was found to be an adequate approximation to the simulated phase covariance.

The generalized expressions for the Cramer-Rao lower bound given in Sec. 3 were developed under the assumption of zero mean, Gaussian distributed noise (i.e., a thermal-noise-limited detector). The lower bound expression for the shearing interferometer in Sec. 4 was developed first for Gaussian distributed noise. An interpretation of that expression was then given to treat the case of Poisson distributed noise (i.e., a shot-noise-limited detector). In the simulation of the shearing interferometer, Gaussian distributed noise was used.

The shearing interferometer was simulated by using a discrete version of Eqs. (2) and (23). Uncorrelated, zero mean, Gaussian distributed noise was added, and the four measurements in each of the two shear directions were combined to give the tangents of the phase differences in each direction.[9] The successive overrelaxation algorithm was used to give the least mean-squared error phase estimate.[10] An initial phase estimate for the algorithm was determined by simple two-dimensional integration of the (noisy) phase difference data.

Figure 4 shows a comparison of the Cramer-Rao lower bounds to a number of simulation results as a function of P_c for $\sigma_\phi = \pi/2$ and $d = r_\phi/6$. The lower bound is approached asymptotically as the light level increases (at higher signal-to-noise ratio). This implies that the Cramer-Rao lower bound is a useful predictor of actual shearing interferometer performance.

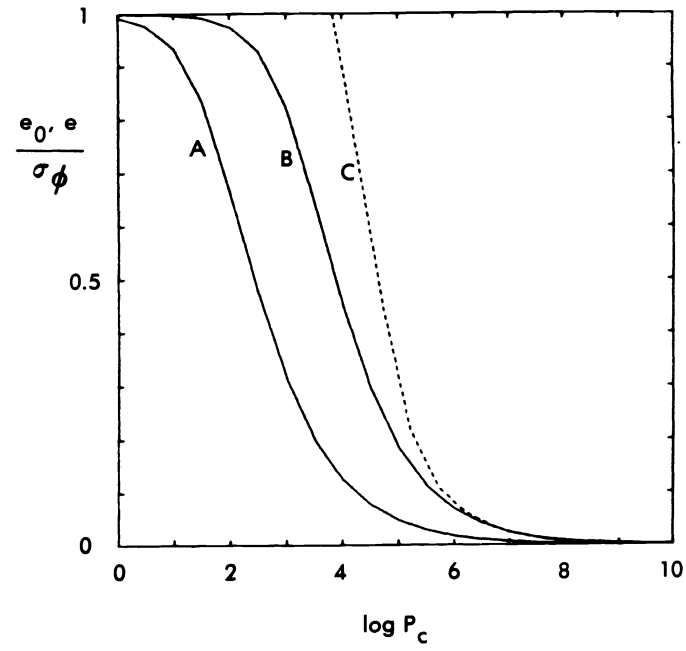

Fig. 4. Comparison of shearing interferometer lower bounds to simulation phase estimate error versus light level P_c for point object and $\sigma_\phi = \pi/2$. Curves (A) and (B) show lower bounds for shear distances $d = r_\phi$ (optimum) and $r_\phi/6$, respectively. Curve (C) shows simulation errors to be compared with curve (B). The simulation error approaches the lower bound as light level P_c increases.

6. CONCLUSION

The Cramer-Rao method for finding a lower bound on estimation error was applied to a wavefront sensor. In addition to an analysis of the general case, the investigation was pursued to numerical computation of the shearing interferometer error lower bound. To investigate the usefulness of the Cramer-Rao error bounds in predicting sensor performance, the shearing interferometer sensor was numerically simulated, and an appropriate algorithm was used to obtain a phase estimate. The error lower bound and the computer simulation error for the shearing interferometer sensor are given in Fig. 4 for a point object and atmospheric phase variance $\sigma_\phi = \pi/2$.

As shown, both the lower bound and the simulation errors decrease as the number of photons per coherence cell P_c (i.e., the light level) increases. The simulation error approaches the lower bound asymptotically as P_c increases. This implies that the Cramer-Rao lower bound can be used to predict wavefront sensor performance at least at the higher light levels.

The results described above encourage further research in the application of the Cramer-Rao lower bound to the evaluation of wavefront sensors. Recommended research efforts are (1) development of methods for solving the integral equation [Eq. (9)] for the inverse information kernel in cases where the Fourier domain solution is not applicable, and (2) study of cases in which the extended object is coherent or partially coherent rather than incoherent, as was assumed here.

7. REFERENCES

1. M. Born and E. Wolf, *Principles of Optics*, p. 526, Pergamon, Oxford (1975).
2. S. R. Robinson, "Fundamental performance limitations for the phase retrieval problem," in *Wavefront Sensing*, N. Bareket and C. L. Koliopoulos, eds., Proc. SPIE 351, 66 (1983).
3. H. L. Van Trees, "Bounds on the accuracy attainable in the estimation of continuous random processes," IEEE Trans. Inf. Theory IT-12(3), 298 (1966).
4. H. L. Van Trees, *Detection, Estimation and Modulation Theory, Part I*, pp. 66–73, 79–85, 437–441, Wiley, New York (1968).
5. D. L. Fried, "Statistics of a geometric representation of wavefront distortion," J. Opt. Soc. Am. 55(11), 1427 (1965).
6. R. E. Hufnagel, "Propagation through atmospheric turbulence," in *The Infrared Handbook*, W. L. Wolfe and G. J. Zissis, eds., pp. 6-7, 6-28 through 6-31, Office of Naval Research, Washington (1978).

7. J. C. Wyant, "Double frequency grating lateral shear interferometer," Appl. Opt. 12(9), 2057 (1973).
8. J. C. Wyant, "White light extended source shearing interferometer," Appl. Opt. 13(1), 200 (1974).
9. J. C. Wyant, "Use of an ac heterodyne lateral shear interferometer with real-time wavefront correction systems," Appl. Opt. 14(11), 2622 (1975).
10. W. H. Southwell, "Wavefront estimation from wavefront slope measurements," J. Opt. Soc. Am. 70(8), 998 (1980).
11. B. L. McGlamery, "Computer simulation studies of compensation of turbulence degraded images," in *Image Processing*, J. C. Urbach, ed., Proc. SPIE 74, 225 (1976).

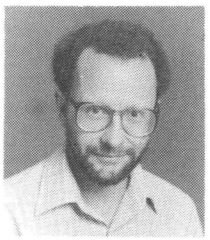

Jack Cederquist was born in Pasadena, Calif., on May 29, 1948. He received the B.A. degree in physics (magna cum laude) from Pomona College, Claremont, Calif., in 1970 and the M.S. and Ph.D. degrees in electrical engineering from the University of California, San Diego, in 1977 and 1980, respectively.

His graduate research concentrated on the use of optical feedback techniques to expand the capabilities of optical information processors. He joined the Environmental Research Institute of Michigan in 1981 and has been involved in research in novel sensor designs and data processing methods, holographic optical element design, computer-generated holography, and hybrid processors that combine optical, digital, and video methods.

Dr. Cederquist is a member of SPIE, OSA, IEEE, and Phi Beta Kappa.

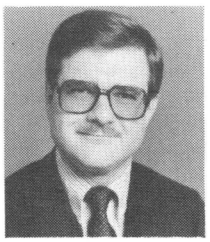

Stanley R. Robinson was born in Akron, Ohio, on July 24, 1949. He received BSEE and MSEE degrees from the University of Akron in 1971 and 1972, respectively, and a Ph.D. degree in electrical engineering from the Massachusetts Institute of Technology, Cambridge, Mass., in June 1975.

From 1972 to early 1980, he was with the Electrical Engineering Department of the Air Force Institute of Technology, where he developed a graduate curriculum in signal processing for electro-optics systems and conducted research in applying detection, estimation, and modulation theory to the design and performance specification of systems that use signals at optical frequencies. He received the USAF Research and Development Award (1976) for his research efforts in electro-optics systems.

Since 1980, he has been employed at the Environmental Research Institute of Michigan. He is currently the Director of Advanced Technology Programs within the Infrared and Optics Division and is responsible for the development of research programs that deal with new sensing and data processing technologies. His research interests include wavefront sensing from intensity measurements, design of optimum modulation frequencies for laser sensors, and nonconventional imaging techniques.

Dr. Robinson is a member of Omicron Delta Kappa, Eta Kappa Nu, Sigma Xi, Tau Beta Pi, OSA, and IEEE.

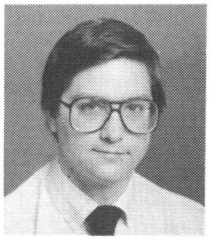

David Kryskowski was born in Detroit, Mich., in 1956. He received the B.S. degree in electrical engineering from the University of Michigan, Ann Arbor, Mich., in 1979 and the M.S. degree in electrical engineering from Wayne State University, Detroit, Mich., in 1983.

Since 1983 he has been a member of the research staff at the Environmental Research Institute of Michigan. He is currently working in the area of infrared image processing.

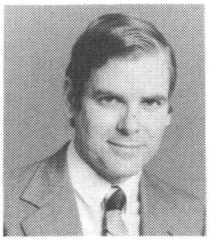

James R. Fienup was born in St. Louis, Mo., on April 17, 1948. He received B.A. degrees in physics and mathematics (magna cum laude) from Holy Cross College, Worcester, Mass., in 1970 and M.S. and Ph.D. degrees in applied physics from Stanford University in 1972 and 1975, respectively.

His graduate work was concerned with a new type of computer-generated hologram. In 1975 he joined the Environmental Research Institute of Michigan, where he is currently head of the information processing section of the Electro-Optics Department. His research activities include phase retrieval and image reconstruction algorithms, optical and digital image processing, and holographic optical elements.

Dr. Fienup is a member of SPIE, OSA, IEEE, and Sigma Xi. He is the recipient of SPIE's 1979 Rudolph Kingslake Medal and Prize and the ICO's 1983 International Prize in Optics. He was an Associate Editor of Optics Letters (1983-85) and feature editor of JOSA (Nov. 1983). He is the chairman of the OSA topical meeting on Signal Recovery and Synthesis II, Honolulu, Hawaii, April 1986.

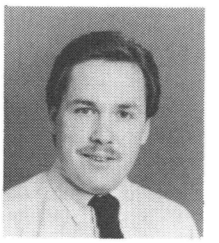

Christopher C. Wackerman was born in Rochester, N.Y., on Dec. 11, 1959. He received the B.S. degree in mathematics, the B.S.E. degree in computer science, and the M.S. degree in computer science from the University of Michigan, Ann Arbor, Mich., in 1981, 1982, and 1983, respectively.

He joined the Environmental Research Institute of Michigan in 1982 and is currently working on synthetic aperture radars and signal processing.